

Supplementary Information

Discovery of a kernel for controlling biomolecular regulatory networks

Junil Kim, Sang-Min Park, and Kwang-Hyun Cho*

Department of Bio and Brain Engineering, Korea Advanced Institute of Science and Technology
(KAIST), Daejeon 305-701, Republic of Korea

*Corresponding author, E-mail: ckh@kaist.ac.kr, Phone: +82-42-350-4325, Fax: +82-42-350-4310, Web: <http://sbie.kaist.ac.kr/>.

Contents

I. Supplementary Methods

II. Supplementary Figures

Supplementary Figure S1. Relationship between the size of control kernel and the topological characteristics in the eight bimolecular regulatory networks.

Supplementary Figure S2. Relationship between the size of control kernel and the topological characteristics in random networks.

Supplementary Figure S3. The average size of control kernel in the random networks with respect to the number of attractors and the proportion of basin size of the primary attractor.

Supplementary Figure S4. The average number of attractors and the proportion of basin size of the primary attractor in the random networks with respect to the proportion of inhibitory links.

Supplementary Figure S5. Topological and dynamical characteristics of the control kernel nodes in the eight biomolecular regulatory networks.

Supplementary Figure S6. Topological and dynamical properties of the control kernel nodes in the random networks.

Supplementary Figure S7. The enrichment of drug targets and chemical-binding interactions in the control kernel nodes and the driver nodes in the human fibroblast signaling network.

Supplementary Figure S8. The flow diagram illustrating the control kernel identification algorithm.

Supplementary Figure S9. Average fitness trajectories during the artificial evolution of chromosomes for the identification of control kernel in the eight biomolecular regulatory networks.

III. Supplementary Tables

Supplementary Table S1. State coherency and attractor states of the *Saccharomyces cerevisiae* cell cycle network.

Supplementary Table S2. State coherency and attractor states of the *Schizosaccharomyces pombe* cell cycle network.

Supplementary Table S3. State coherency and attractor states of the GRN underlying mammalian cortical area development.

Supplementary Table S4. State coherency and attractor states of the GRN underlying *Arabidopsis thaliana* development.

Supplementary Table S5. State coherency and attractor states of the GRN underlying mouse myeloid development.

Supplementary Table S6. State coherency and attractor states of the mammalian cell cycle network.

Supplementary Table S7. State coherency and primary attractor states of the CREB signaling network.

Supplementary Table S8. State coherency and primary attractor states of the human fibroblast signaling network.

Supplementary Table S9. Comparison of the control kernel, driver node set, driver node set on switchboard dynamics (SBD), and optimal sensor set of the human fibroblast signaling network.

IV. Supplementary References

I. Supplementary Methods

Parameters of the genetic algorithm (GA)

For the GA employed in the control kernel identification algorithm (Fig. S8), different values of N (the number of chromosomes) and M (generations for artificial evolution) were used depending on the network to ensure the convergence of average fitness for each chromosome: $N=100$ and $M=100$ for the *S. cerevisiae* cell cycle network, the *S. pombe* cell cycle network, the GRN underlying mammalian cortical area development, the GRN underlying *A. thaliana* development, the GRN underlying mouse myeloid development, and the mammalian cell cycle network; $N=1000$ and $M=100$ for the CREB signaling network; $N=100$ and $M=2000$ for the human fibroblast signaling network; and $N=100$ and $M=100$ for random networks. Mutation rate 0.01 and crossover rate 0.68 (1) were used.

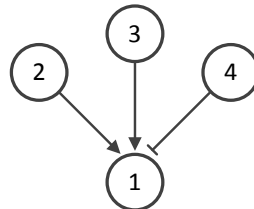
Boolean network model based on four different types of logical rules for state transition

We obtained the state transition diagram of each random network by simultaneously updating the Boolean functions based on four different types of logical rules (Rule 1~4). In Rule 1 adopted from Li *et al.* (2), the state of a node in the next time step depends on the present network states as follows:

$$x_i(t+1) = \begin{cases} 1, & \sum_j a_{ij}x_j(t) > 0 \\ 0, & \sum_j a_{ij}x_j(t) < 0 \\ x_i(t), & \sum_j a_{ij}x_j(t) = 0 \end{cases} ,$$

where $x_i(t)$ denotes the state of node i at time step t , $a_{ij} = 1$ if node j activates node i , $a_{ij} = -1$ if node j inhibits node i , and $a_{ij} = 0$ if node j does not regulate node i . Rule 2 is adopted from Abdi *et al.* (3), where every Boolean logic for activatory link is ‘OR’ whereas every Boolean logic for inhibitory link is ‘AND’. Every Boolean logic is ‘AND’ in Rule 3 while every Boolean logic is ‘OR’ in Rule 4.

For instance, let us consider the following toy example network where node 2 and node 3 activate node 1 and node 4 inhibits node 1.



According to Rule 1, the state of node 1 at time step $t+1$ is determined by the states of node 1, 2, 3, and 4 at time step t as follows:

$x_1(t)$	$x_2(t)$	$x_3(t)$	$x_4(t)$	$x_1(t+1)$
0	0	0	0	0

0	0	0	1	0
0	0	1	0	1
0	0	1	1	0
0	1	0	0	1
0	1	0	1	0
0	1	1	0	1
0	1	1	1	1
1	0	0	0	1
1	0	0	1	0
1	0	1	0	1
1	0	1	1	1
1	1	0	0	1
1	1	0	1	1
1	1	1	0	1
1	1	1	1	1
1	1	1	1	1

According to Rule 2, the state of node 1 at time step $t+1$ is determined by the states of node 2, 3, and 4 at time step t as follows:

$x_2(t)$	$x_3(t)$	$x_4(t)$	$x_1(t+1)$
0	0	0	0
0	0	1	0
0	1	0	1
0	1	1	0
1	0	0	1
1	0	1	0
1	1	0	1
1	1	1	0
0	0	0	0
0	0	1	0

According to Rule 3, the state of node 1 at time step $t+1$ is determined by the states of node 2, 3, and 4 at time step t as follows:

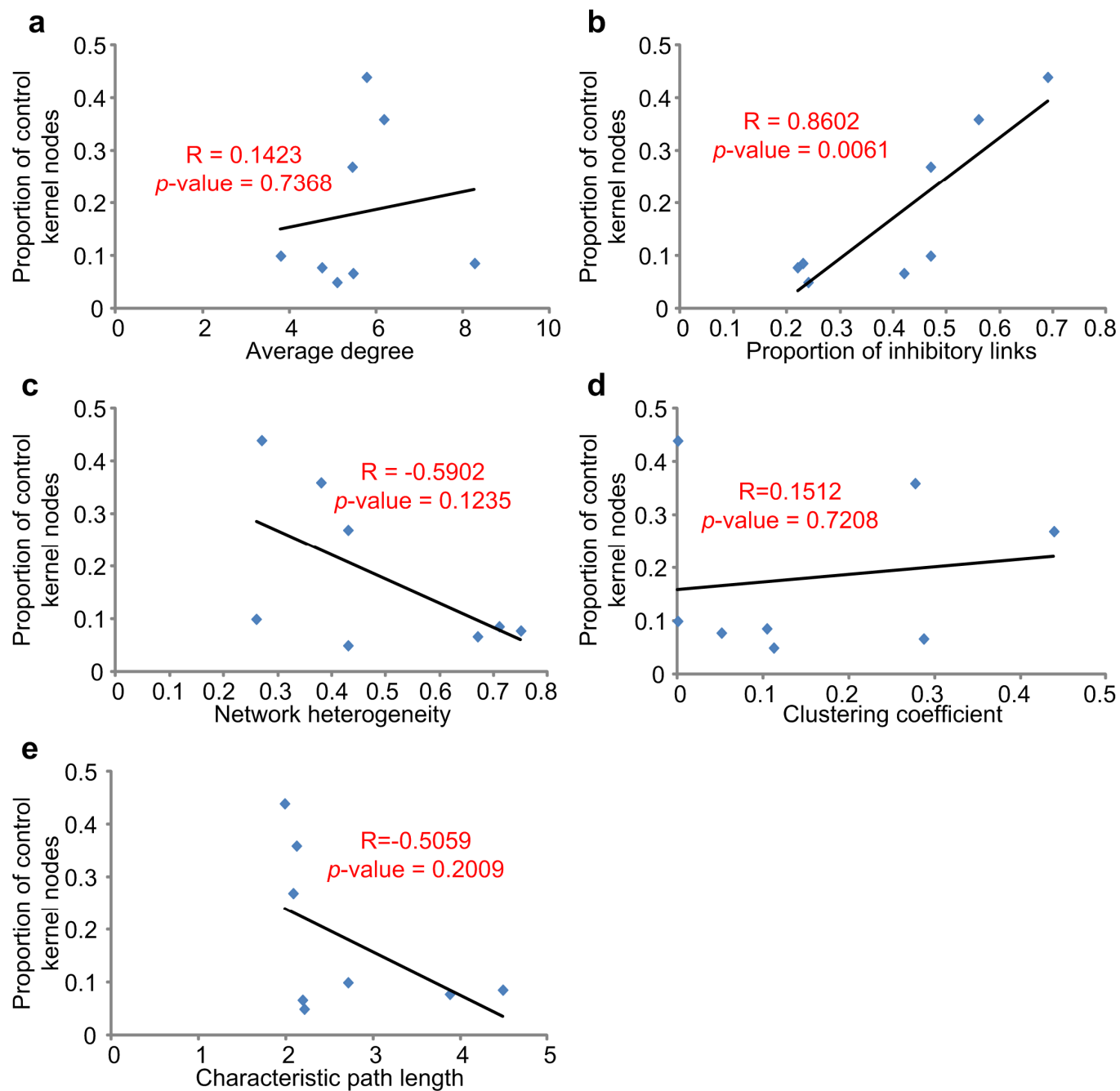
$x_2(t)$	$x_3(t)$	$x_4(t)$	$x_1(t+1)$
0	0	0	0
0	0	1	0
0	1	0	0
0	1	1	0
1	0	0	0
1	0	1	0
1	1	0	1

1	1	1	0
0	0	0	0
0	0	1	0

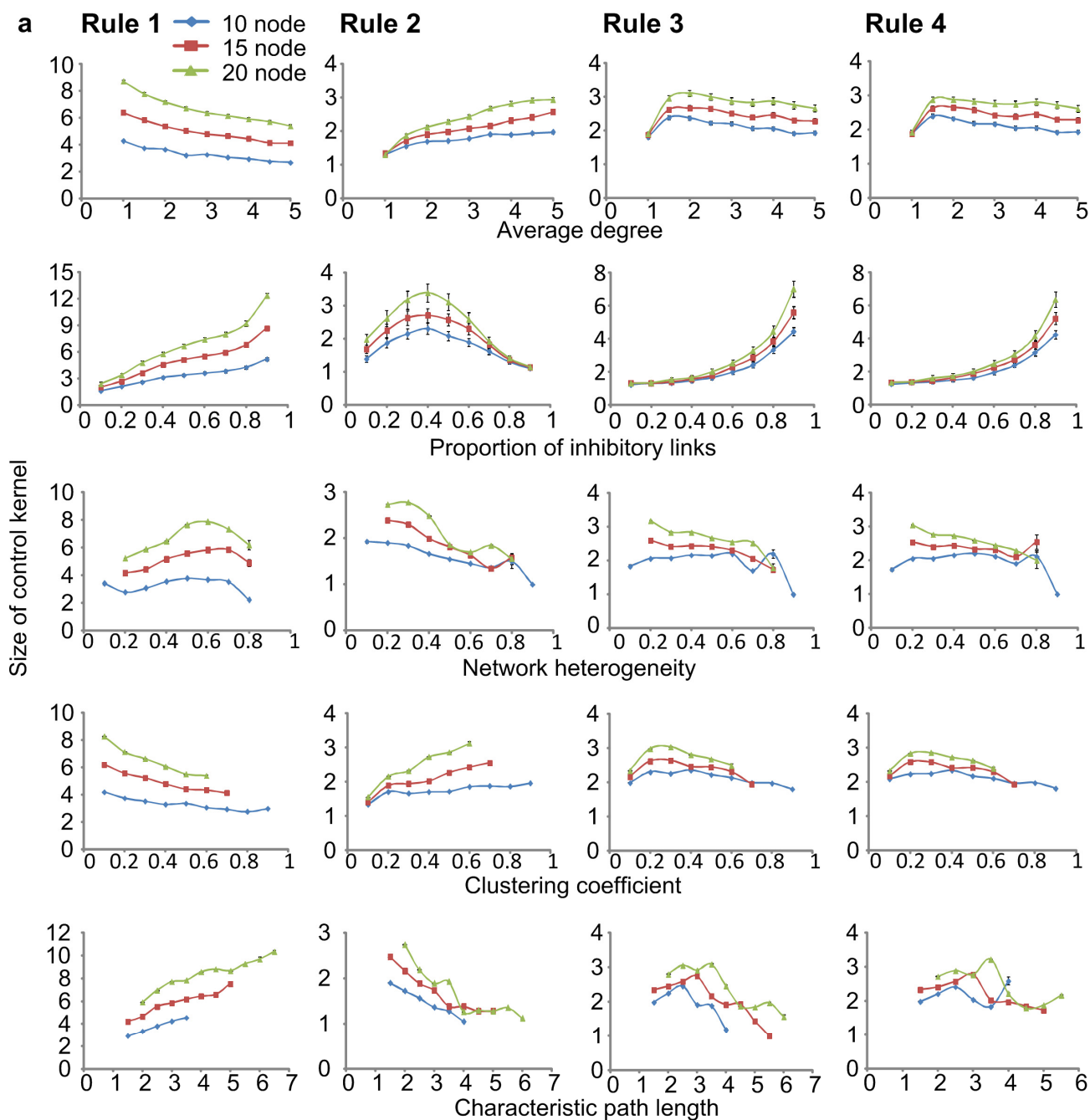
According to Rule 4, the state of node 1 at time step $t+1$ is determined by the states of node 2, 3, and 4 at time step t as follows:

$x_2(t)$	$x_3(t)$	$x_4(t)$	$x_1(t+1)$
0	0	0	1
0	0	1	0
0	1	0	1
0	1	1	1
1	0	0	1
1	0	1	1
1	1	0	1
1	1	1	1
0	0	0	1
0	0	1	1

II. Supplementary Figures



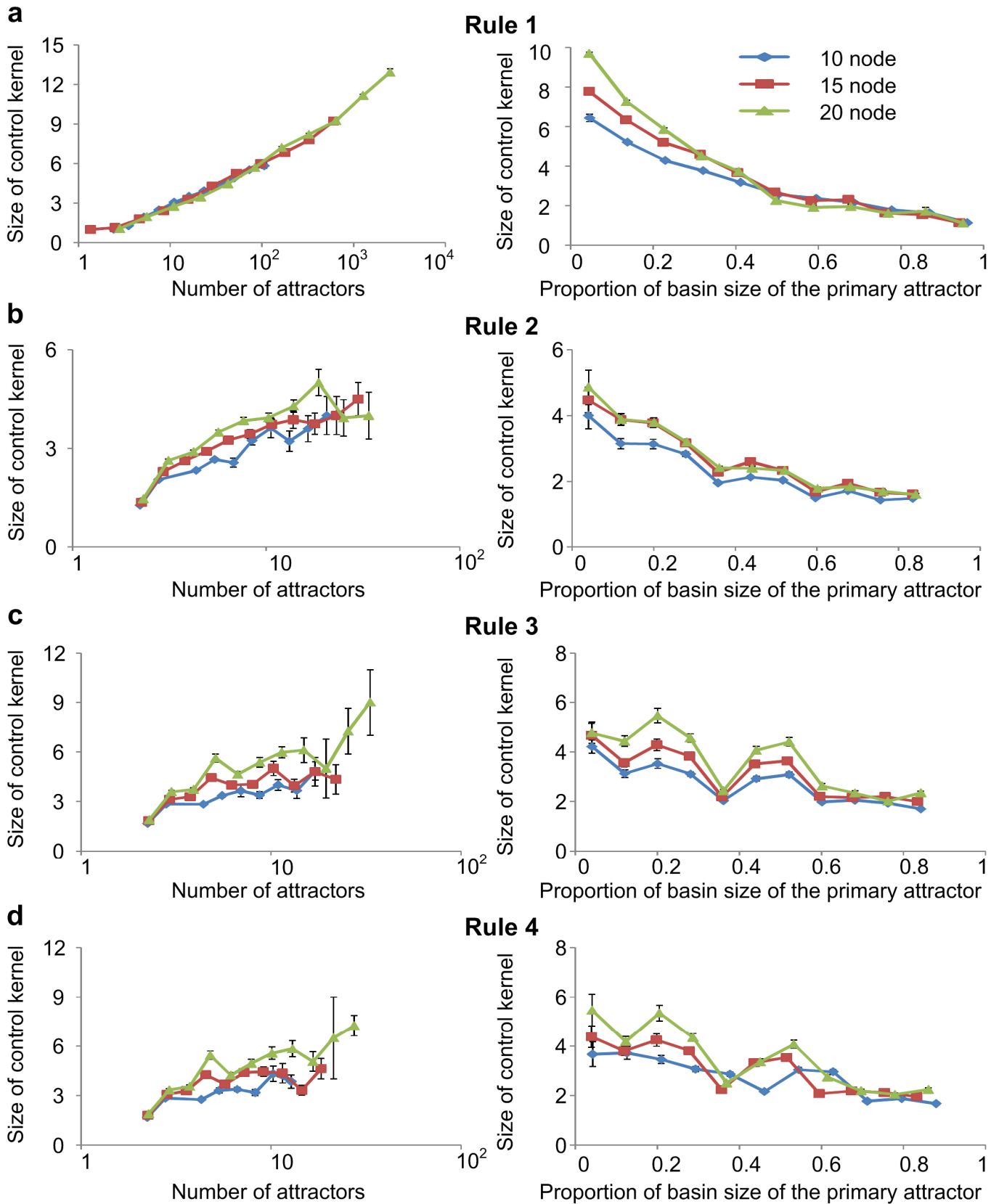
Supplementary Figure S1. Relationship between the size of control kernel and the topological characteristics in the eight bimolecular regulatory networks. (a) Average degree. (b) Proportion of inhibitory links. (c) Network heterogeneity. (d) Clustering coefficient. (e) Characteristic path length. R denotes Pearson's correlation coefficient.



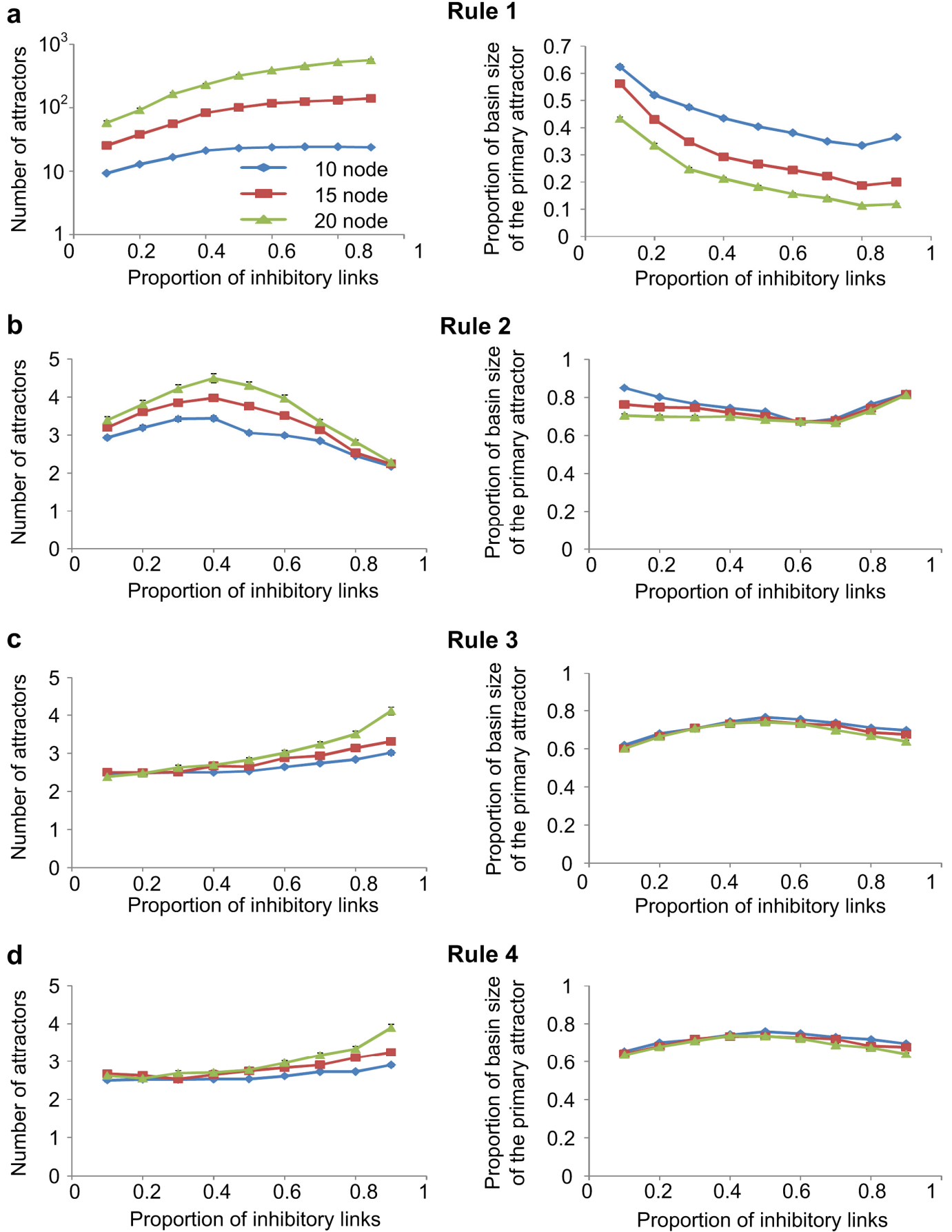
b

Pearson's correlation coefficient	Rule 1			Rule 2			Rule 3			Rule 4		
	10 node	15 node	20 node	10 node	15 node	20 node	10 node	15 node	20 node	10 node	15 node	20 node
Average degree	-0.283	-0.268	-0.272	0.166	0.225	0.253	-0.043	-0.000	0.027	-0.049	0.001	0.033
Proportion of inhibitory links	0.613	0.733	0.783	-0.158	-0.191	-0.224	0.563	0.554	0.557	0.520	0.503	0.514
Network heterogeneity	0.198	0.207	0.210	-0.129	-0.164	-0.200	-0.024	-0.028	-0.044	0.026	-0.027	-0.050
Clustering coefficient	-0.263	-0.247	-0.260	0.147	0.217	0.243	-0.033	0.001	0.031	-0.047	-0.005	0.031
Characteristic path length	0.285	0.261	0.268	-0.163	-0.207	-0.241	0.008	-0.045	-0.079	0.024	-0.041	-0.074

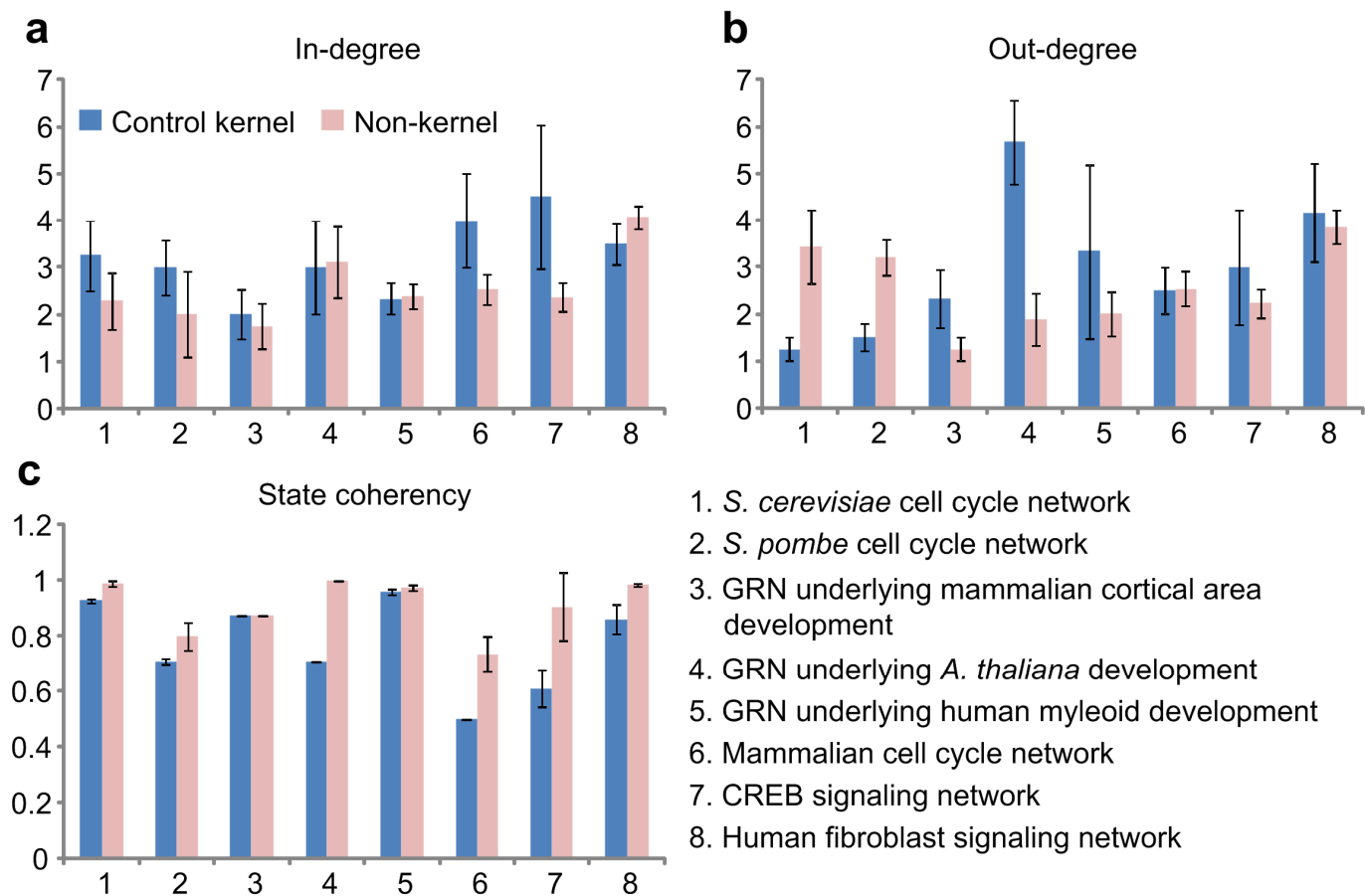
Supplementary Figure S2. Relationship between the size of control kernel and the topological characteristics in random networks. (a) Graphs for the average size of control kernel with respect to the five topological parameters (average degree, the proportion of inhibitory links, network heterogeneity, clustering coefficient, and characteristic path length). (b) Pearson's correlation coefficients between the size of control kernel and each of the five topological parameters. Here the correlation coefficients greater than 0.5 are marked in red.



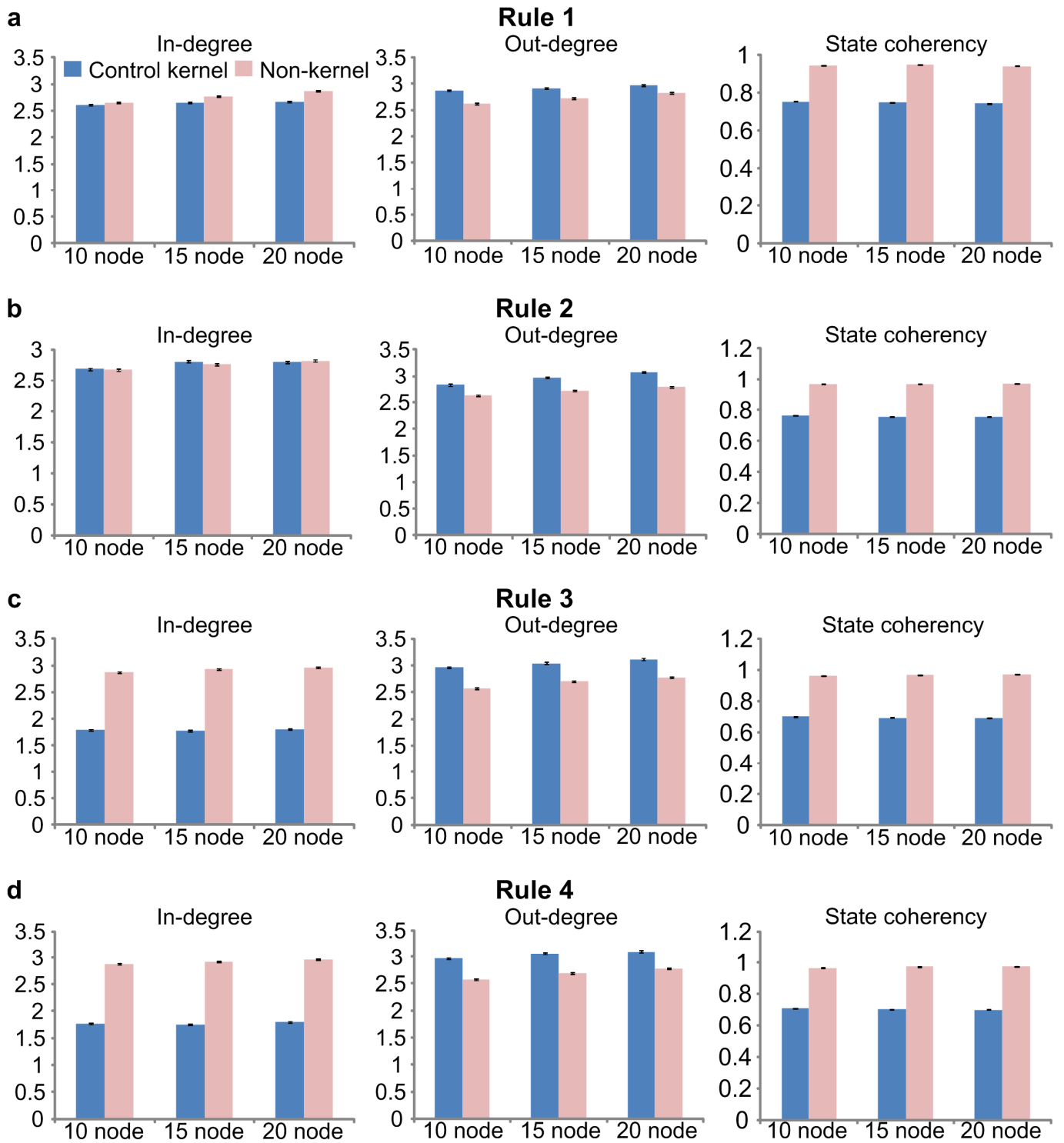
Supplementary Figure S3. The average size of control kernel in the random networks with respect to the number of attractors and the proportion of basin size of the primary attractor. (a) Rule 1. (b) Rule 2. (c) Rule 3. (d) Rule 4.



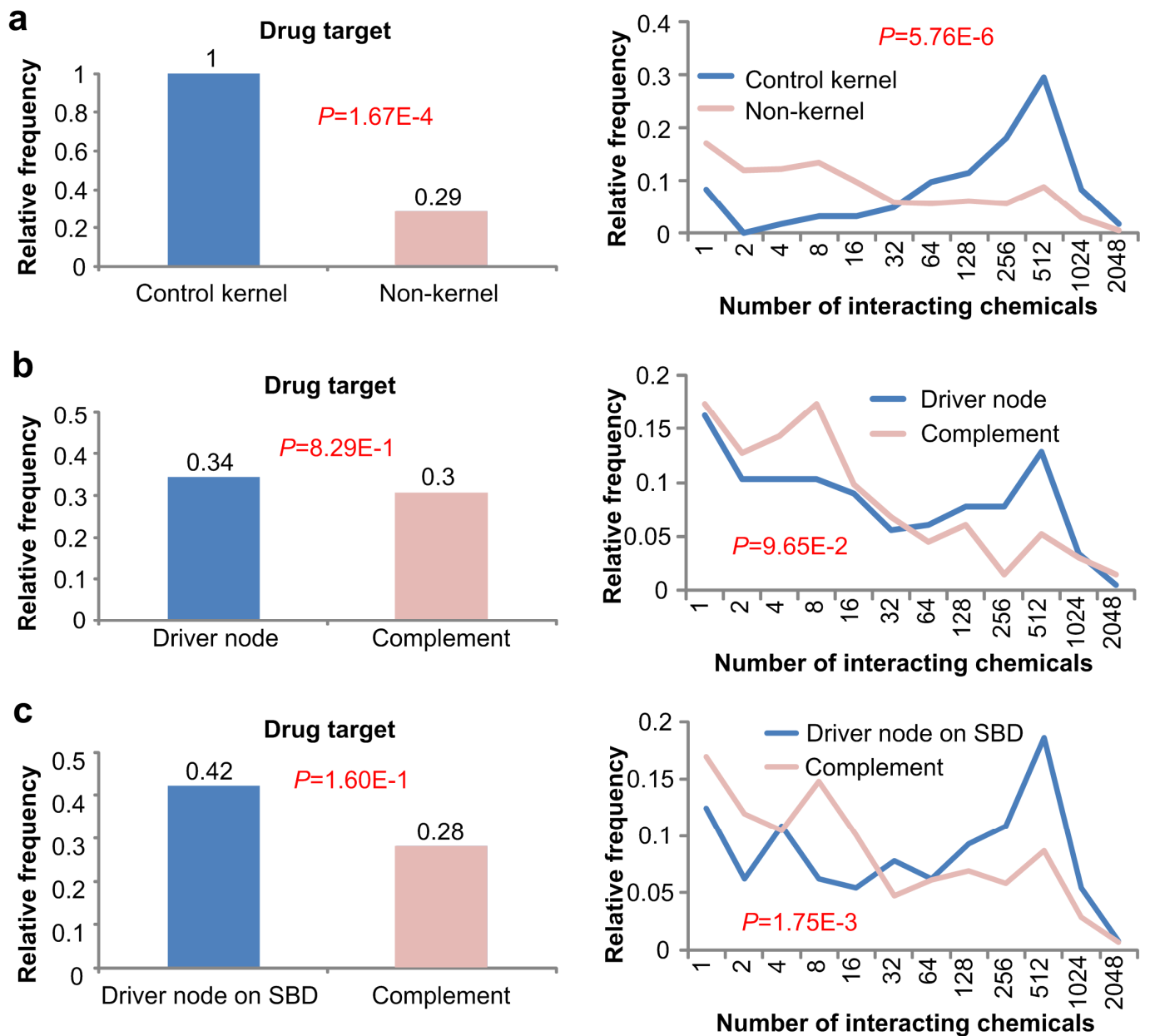
Supplementary Figure S4. The average number of attractors and the proportion of basin size of the primary attractor in the random networks with respect to the proportion of inhibitory links. (a) Rule 1. (b) Rule 2. (c) Rule 3. (d) Rule 4.



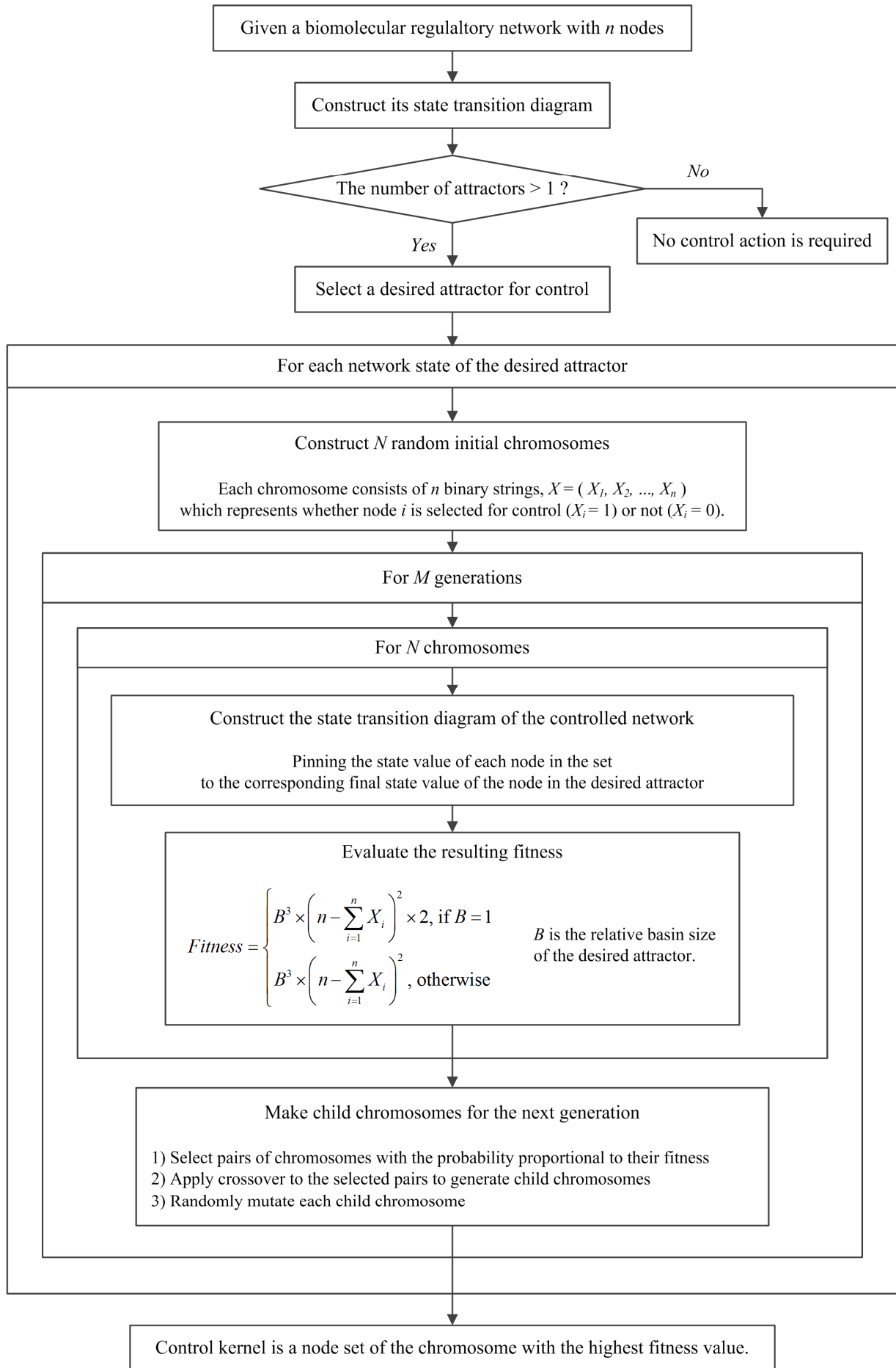
Supplementary Figure S5. Topological and dynamical characteristics of the control kernel nodes in the eight biomolecular regulatory networks. (a) In-degree (the number of incoming links). (b) Out-degree (the number of out-going links). (c) State coherency.



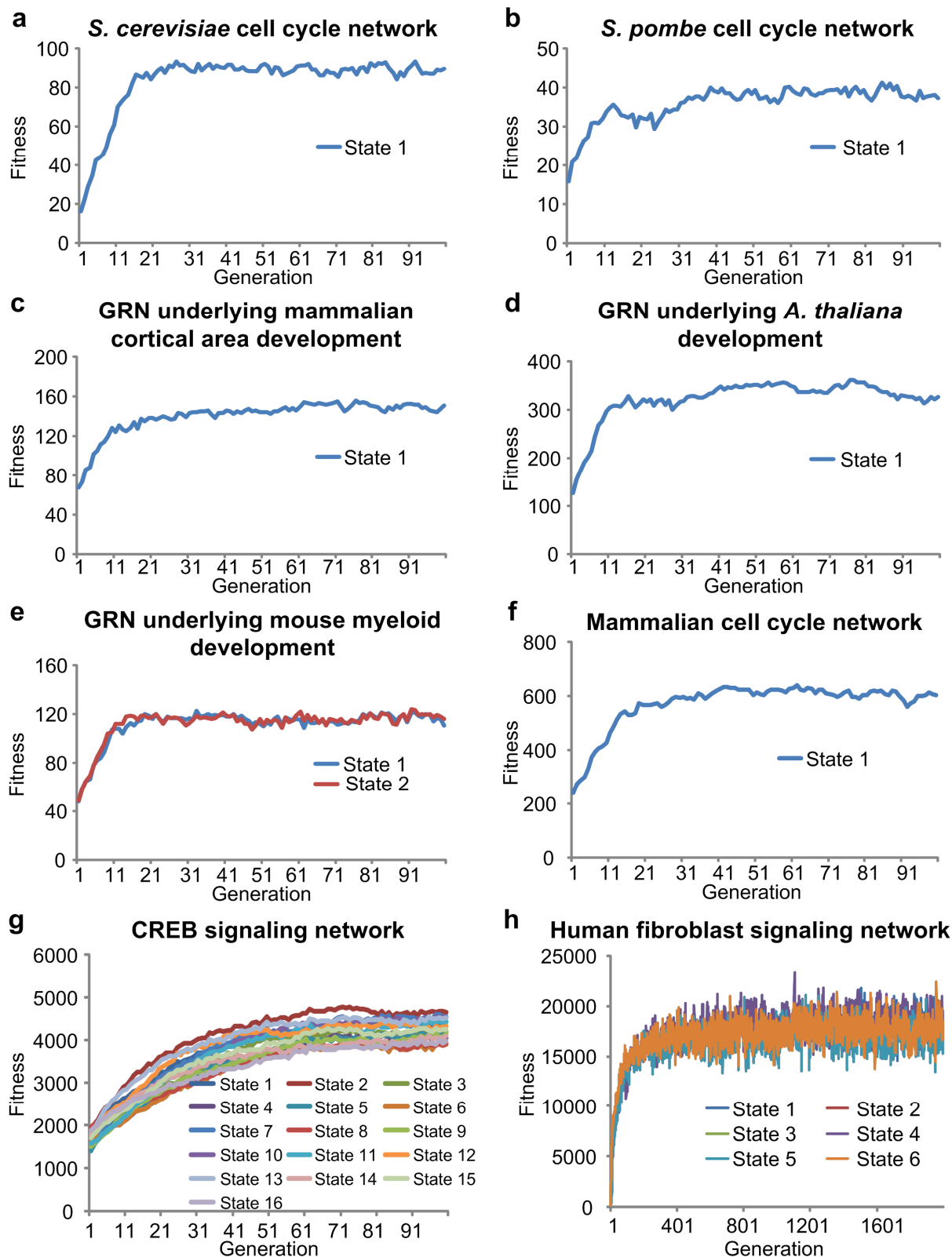
Supplementary Figure S6. Topological and dynamical properties of the control kernel nodes in the random networks. In-degree, out-degree, and state coherency of the control kernel nodes and non-kernel nodes in the random networks with four different logical rules. (a) Rule 1. (b) Rule 2. (c) Rule 3. (d) Rule 4.



Supplementary Figure S7. The enrichment of drug targets and chemical-binding interactions in the control kernel nodes and the driver nodes in the human fibroblast signaling network. (a, b) Control kernel nodes. (c, d) Driver nodes. (e, f) Driver nodes on switchboard dynamics (SBD).



Supplementary Figure S8. The flow diagram illustrating the control kernel identification algorithm.



Supplementary Figure S9. Average fitness trajectories during the artificial evolution of chromosomes for the identification of control kernel in the eight biomolecular regulatory networks. (a) *Saccharomyces cerevisiae* cell cycle network. (b) *Schizosaccharomyces pombe* cell cycle network. (c) The GRN underlying mammalian cortical area development. (d) The GRN underlying *Arabidopsis thaliana* development. (e) The GRN underlying mouse myeloid development. (f) Mammalian cell cycle network. (g) CREB signaling network. (h) The human fibroblast signaling network. ‘State’ in the legend of each figure denotes the respective network state of the desired attractor. The desired attractors of (e), (g), and (h) are cyclic attractors with the period length greater than two.

III. Supplementary Tables

Supplementary Table S1. State coherency and attractor states of the *Saccharomyces cerevisiae* cell cycle network. The control kernel nodes are marked in red and the number in the parenthese denotes the basin size of the corresponding attractor. The control kernel of the *Saccharomyces cerevisiae* cell cycle network is {Cdh1, MBF, SBF, Sic1}.

Node name	Cdc20_Cdc14	Cdh1	Clb1_2	Clb5_6	Cln1_2	Cln3	MBF	Mcm1_SFF	SBF	Sic1	Swi5
State coherency	1	0.915	1	1	0.926	1	0.943	1	0.926	0.922	1
Attractor 1 (1764)	0	1	0	0	0	0	0	0	0	1	0
Attractor 2 (151)	0	0	0	0	1	0	0	0	1	0	0
Attractor 3 (109)	0	1	0	0	0	0	1	0	0	1	0
Attractor 4 (9)	0	0	0	0	0	0	0	0	0	1	0
Attractor 5 (7)	0	0	0	0	0	0	0	0	0	0	0
Attractor 6 (7)	0	0	0	0	0	0	1	0	0	1	0
Attractor 7 (1)	0	1	0	0	0	0	0	0	0	0	0

Supplementary Table S2. State coherency and attractor states of the *Schizosaccharomyces pombe* cell cycle network. The control kernel nodes are marked in red and the number in the parenthese denotes the basin size of the corresponding attractor. The control kernel of the *Schizosaccharomyces pombe* cell cycle network is {Cdc25, Rum1, Ste9, Wee1}.

Node name	Cdc2/13	Cdc2/13*	Cdc25	PP	Rum1	SK	Slp1	Ste9	Wee1
State coherency	0.75	0.75	0.723	0.75	0.693	1	0.75	0.693	0.723
Attractor 1 (341)	0	0	0	0	1	0	0	1	1
Attractor 2 (128)	1	1	1	1	0	0	1	0	0
Attractor 3 (9)	0	0	0	0	0	0	0	0	1
Attractor 4 (6)	0	0	0	0	0	0	0	0	0
Attractor 5 (6)	0	0	1	0	0	0	0	0	1
Attractor 6 (5)	0	0	0	0	0	0	0	1	1
Attractor 7 (5)	0	0	0	0	1	0	0	0	1
Attractor 8 (2)	0	0	0	0	1	0	0	1	0
Attractor 9 (2)	0	0	1	0	1	0	0	1	0
Attractor 10 (2)	0	0	1	0	1	0	0	1	1
Attractor 11 (1)	0	0	0	0	0	0	0	1	0
Attractor 12 (1)	0	0	0	0	1	0	0	0	0
Attractor 13 (1)	0	0	1	0	0	0	0	1	0
Attractor 14 (1)	0	0	1	0	0	0	0	1	1
Attractor 15 (1)	0	0	1	0	1	0	0	0	0
Attractor 16 (1)	0	0	1	0	1	0	0	0	1

Supplementary Table S3. State coherency and attractor states of the GRN underlying mammalian cortical area development. The control kernel nodes are marked in red and the number in the parenthese denotes the basin size of the corresponding attractor. The control kernels of the GRN underlying mammalian cortical area development are {Fgf8_g}, {Emx2_g}, {Sp8_g}, {Fgf8_p}, {Emx2_p}, and {Sp8_p}.

Node name	Fgf8_g	Emx2_g	Pax6_g	Coup_g	Sp8_g	Fgf8_p	Emx2_p	Pax6_p	Coup_p	Sp8_p
State coherency	0.875	0.875	0.875	0.875	0.875	0.875	0.875	0.875	0.875	0.875
Attractor 1 (784)	0	1	0	1	0	0	1	0	1	0
Attractor 2 (224)	0	1	0	1	0	1	0	1	0	1
	1	0	1	0	1	0	1	0	1	0
Attractor 3 (16)	1	0	1	0	1	1	0	1	0	1

Supplementary Table S4. State coherency and attractor states of the GRN underlying *Arabidopsis thaliana* development. The control kernel nodes are marked in red and the number in the parenthese denotes the basin size of the corresponding attractor. The control kernels of the GRN underlying *Arabidopsis thaliana* development are {API}, {LFY}, and {SEP}.

Node name	AG	API	AP2	AP3	CLF	EMF1	FT	FUL	LFY	LUG	PI	SEP	TFL1	UFO	WUS
State coherency	1	0.71	1	1	1	1	1	1	0.71	1	1	0.71	1	1	1
Attractor 1 (23200)	0	1	0	1	0	0	0	0	1	0	1	1	0	0	0
Attractor 2 (9480)	0	0	0	1	0	0	0	0	0	0	1	0	0	0	0
Attractor 3 (88)	0	0	0	0	0	0	0	0	0	0	0	0	0	0	0

Supplementary Table S5. State coherency and attractor states of the GRN underlying mouse myeloid development. The control kernel nodes are marked in red and the number in the parenthese denotes the basin size of the corresponding attractor. The control kernels of the GRN underlying mouse myeloid development are {GATA_1, EKLF, Fli_1} and {EKLF, Fli_1, PU1}.

Node name	GATA_2	GATA_1	FOG_1	EKLF	Fli_1	SCL	CEBPA	PU1	cJun	EgrNab	Gfi_1
State coherency	1	0.9313	0.9313	0.9641	0.9641	0.9344	0.9813	0.9781	0.993	0.993	0.982
Attractor 1 (1088)	0	1	1	1	1	1	0	0	0	0	0
	0	1	1	0	0	1	0	0	0	0	0
Attractor 2 (240)	0	0	0	0	0	0	1	1	0	0	1
Attractor 3 (192)	0	0	0	0	0	0	0	0	0	0	0
Attractor 4 (128)	0	0	0	0	0	0	0	1	1	1	0
Attractor 5 (128)	0	1	0	0	0	0	1	1	0	0	1
	0	0	1	1	1	0	1	0	0	0	1
Attractor 6 (128)	0	1	1	0	1	1	0	0	0	0	0
Attractor 7 (128)	0	1	1	1	0	1	0	0	0	0	0
Attractor 8 (16)	0	0	0	0	0	0	1	1	1	1	0

Supplementary Table S6. State coherency and attractor states of the mammalian cell cycle network. The control kernel nodes are marked in red and the number in the parentheses denotes the basin size of the corresponding attractor. The control kernels of the mammalian cell cycle network are {MEK1} and {IGF1R}.

Node name	State coherency	Attractor 1 (9984)	Attractor 2 (16)
Akt1	0.5008	1	0
CDK2	0.5008	1	0
CDK4	0.5008	1	0
CDK6	0.5008	1	0
cMYC	0.5008	1	0
CycD1	0.5008	1	0
CycE1	0.5008	1	0
Era	0.5008	1	0
ErbB1	1	0	0
ErbB1_2	1	0	0
ErbB1_3	1	0	0
ErbB2	1	0	0
ErbB2_3	1	0	0
ErbB3	1	0	0
IGF1R	0.5008	1	0
MEK1	0.5008	1	0
p21	1	0	0
p27	1	0	0
pRB	0.5008	1	0
EGF	1	0	0

Supplementary Table S7. State coherency and primary attractor states of the CREB signaling network. The control kernel nodes are marked in red and the number in the parentheses denotes the basin size of the corresponding attractor. The control kernels of the CREB signaling network are {AC2, AC5, Calmodulin, M2R, PKA} and {CREB, CaMKI, Calmodulin, Galphai, PKA}.

Node name	State coherency	Attractor 1 (0.2925)															
5-HT1AR	1	0	0	0	0	0	0	0	0	0	0	0	0	0	0	0	0
5-HT2AR	1	0	0	0	0	0	0	0	0	0	0	0	0	0	0	0	0
5-HT4R	1	0	0	0	0	0	0	0	0	0	0	0	0	0	0	0	0
A1R	1	0	0	0	0	0	0	0	0	0	0	0	0	0	0	0	0
A2AR	1	0	0	0	0	0	0	0	0	0	0	0	0	0	0	0	0
AC1	1	0	0	0	0	0	0	0	0	0	0	0	0	0	0	0	0
AC2	0.5	1	1	0	0	0	1	1	1	0	0	1	1	1	0	0	0

AC5	0.5	1	1	0	0	0	1	1	1	0	0	1	1	1	0	0	0
AKT	1	1	1	1	1	1	1	1	1	1	1	1	1	1	1	1	1
Ach	1	0	0	0	0	0	0	0	0	0	0	0	0	0	0	0	0
Adenosine	1	0	0	0	0	0	0	0	0	0	0	0	0	0	0	0	0
CBP	0.5	0	0	0	1	1	0	0	0	1	1	1	0	0	1	1	1
CREB	0.559	0	1	1	1	0	0	0	1	1	0	0	0	1	1	1	0
CREM	0.787	0	0	0	0	1	0	0	0	0	1	0	0	0	0	0	1
Ca2	0.5	0	1	1	1	0	0	1	1	1	0	0	0	1	1	0	0
CaMKI	0.825	0	0	0	0	0	0	1	0	0	0	0	0	0	0	0	0
CaMKII	0.5	0	0	0	1	1	1	0	0	1	1	1	0	0	0	1	1
CaMKIV	0.787	0	0	0	1	0	0	0	0	1	0	0	0	0	0	1	0
CaMKK	0.825	0	0	0	0	0	1	0	0	0	0	0	0	0	0	0	0
Calmodulin	0.5	0	0	1	1	1	0	0	1	1	1	0	0	0	1	1	0
D1R	1	0	0	0	0	0	0	0	0	0	0	0	0	0	0	0	0
D2R	1	0	0	0	0	0	0	0	0	0	0	0	0	0	0	0	0
D3R	1	0	0	0	0	0	0	0	0	0	0	0	0	0	0	0	0
DAG	1	0	0	0	0	0	0	0	0	0	0	0	0	0	0	0	0
DOR	1	0	0	0	0	0	0	0	0	0	0	0	0	0	0	0	0
Dopamine	1	0	0	0	0	0	0	0	0	0	0	0	0	0	0	0	0
Enkephalin	1	0	0	0	0	0	0	0	0	0	0	0	0	0	0	0	0
GABA	1	0	0	0	0	0	0	0	0	0	0	0	0	0	0	0	0
GABABR	1	0	0	0	0	0	0	0	0	0	0	0	0	0	0	0	0
GSK3	1	0	0	0	0	0	0	0	0	0	0	0	0	0	0	0	0
Galphai	0.5	0	1	1	1	0	0	0	1	1	0	0	0	1	1	1	0
Galphas	1	0	0	0	0	0	0	0	0	0	0	0	0	0	0	0	0
Galphaz	1	0	0	0	0	0	0	0	0	0	0	0	0	0	0	0	0
Gbetagamma	1	1	1	1	1	1	1	1	1	1	1	1	1	1	1	1	1
Glutamate	1	0	0	0	0	0	0	0	0	0	0	0	0	0	0	0	0
Grb2	1	0	0	0	0	0	0	0	0	0	0	0	0	0	0	0	0
ILK	1	1	1	1	1	1	1	1	1	1	1	1	1	1	1	1	1
KOR	1	0	0	0	0	0	0	0	0	0	0	0	0	0	0	0	0
M1R	1	0	0	0	0	0	0	0	0	0	0	0	0	0	0	0	0
M2R	1	0	0	0	0	0	0	0	0	0	0	0	0	0	0	0	0
M4R	1	0	0	0	0	0	0	0	0	0	0	0	0	0	0	0	0
MOR	1	0	0	0	0	0	0	0	0	0	0	0	0	0	0	0	0
N-typeCaCh	1	0	0	0	0	0	0	0	0	0	0	0	0	0	0	0	0
NMDAR	1	0	0	0	0	0	0	0	0	0	0	0	0	0	0	0	0
NOR	1	0	0	0	0	0	0	0	0	0	0	0	0	0	0	0	0
P/QtypeCaCh	0.5	1	1	1	0	0	1	1	1	0	0	0	1	1	0	0	0

PDK1	1	1	1	1	1	1	1	1	1	1	1	1	1	1	1	1	1
PI3K	1	1	1	1	1	1	1	1	1	1	1	1	1	1	1	1	1
PIP2	1	0	0	0	0	0	0	0	0	0	0	0	0	0	0	0	0
PIP3	1	1	1	1	1	1	1	1	1	1	1	1	1	1	1	1	1
PKA	0.5	0	0	1	1	0	0	0	1	1	1	0	0	1	1	1	0
PKC	1	1	1	1	1	1	1	1	1	1	1	1	1	1	1	1	1
PLC β	1	0	0	0	0	0	0	0	0	0	0	0	0	0	0	0	0
PLC γ	1	0	0	0	0	0	0	0	0	0	0	0	0	0	0	0	0
PP2A	1	0	0	0	0	0	0	0	0	0	0	0	0	0	0	0	0
PP2B	0.5	0	0	0	1	1	1	0	0	1	1	1	0	0	0	1	1
RSK	1	1	1	1	1	1	1	1	1	1	1	1	1	1	1	1	1
RasGAP	1	1	1	1	1	1	1	1	1	1	1	1	1	1	1	1	1
SAM68	1	0	0	0	0	0	0	0	0	0	0	0	0	0	0	0	0
Serotonin	1	0	0	0	0	0	0	0	0	0	0	0	0	0	0	0	0
cAMP	0.5	0	1	1	0	0	0	1	1	1	0	0	1	1	1	0	0
cJun	0.5	1	0	0	0	1	1	0	0	0	1	1	1	0	0	1	1
mGluR1	1	1	1	1	1	1	1	1	1	1	1	1	1	1	1	1	1
mGluR7	0.5	1	1	1	0	0	0	1	1	0	0	0	1	1	1	0	0

Supplementary Table S8. State coherency and primary attractor states of the human fibroblast signaling network. The control kernel nodes are marked in red and the number in the parenthese denotes the basin size of the corresponding attractor.

The control kernel of the human fibroblast signaling network is

{DAG, PIP₄, PIP_{2_45}, alpha_{s_R}, Gbg_s, cAMP, Rho, alpha_{q_R}, alpha_{12_13_R}, Raf_{DeP}, PKC_{primed}, Raf_{Loc}}.

Node name	State coherency	Attractor 1 (0.5554)					
EGFR	1	0	0	0	0	0	0
PLC _B	0.948	0	0	0	0	0	0
PLC _g	1	0	0	0	0	0	0
IP3	0.951	0	0	0	0	0	0
DAG	0.845	0	0	0	0	0	0
Ca	0.998	0	0	0	0	0	0
CaM	0.998	0	0	0	0	0	0
CaMKK	0.999	0	0	0	0	0	0
CaMK	0.999	0	0	0	0	0	0
RGS	1	0	0	0	0	0	0
Rap1	1	0	0	0	0	0	0
Shc	1	0	0	0	0	0	0
Grb2	1	0	0	0	0	0	0
Sos	1	0	0	0	0	0	0

Ras	1	0	0	0	0	0	0
PKC	1	0	0	0	0	0	0
AA	0.999	0	0	0	0	0	0
Raf	1	0	0	0	0	0	0
Mek	1	0	0	0	0	0	0
Erk	1	0	0	0	0	0	0
PLA2	0.999	0	0	0	0	0	0
PI3K	0.997	0	0	0	0	0	0
Akt	1	0	0	0	0	0	0
PDK1	0.983	0	0	0	0	0	0
PIP_4	0.500	0	1	0	1	0	1
PIP2_45	0.995	1	1	1	1	1	1
PIP2_34	0.996	0	0	0	0	0	0
PIP3_345	1	0	0	0	0	0	0
PI4K	0.999	1	1	1	1	1	1
PI5K	0.995	1	1	1	1	1	1
alpha_s_R	0.998	0	0	0	0	0	0
Gbg_s	0.870	0	0	0	0	0	0
Gai	0.997	0	0	0	0	0	0
Gas	0.870	0	0	0	0	0	0
Gaq	0.950	0	0	0	0	0	0
GRK	0.771	0	0	0	0	0	0
B_Arrestin	0.916	0	0	0	0	0	0
AC	1	0	0	0	0	0	0
cAMP	0.995	0	0	0	0	0	0
PKA	1	0	0	0	0	0	0
RasGRF_GRP	1	0	0	0	0	0	0
p120RasGAP	0.983	1	1	1	1	1	1
Rho	0.945	0	0	0	0	0	0
RhoGDI	0.996	0	0	0	0	0	0
p190RhoGAP	0.984	0	0	0	0	0	0
p115RhoGEF	1	0	0	0	0	0	0
RhoK	0.945	0	0	0	0	0	0
Fak	1	0	0	0	0	0	0
Cas	1	0	0	0	0	0	0
Src	0.984	0	0	0	0	0	0
Csk	0.984	0	0	0	0	0	0
Myosin	0.944	0	0	0	0	0	0
Actin	1	0	0	0	0	0	0

Integrins	0.998	0	0	0	0	0	0
RKIP	1	0	0	0	0	0	0
Vinc	0.984	0	0	0	0	0	0
Crk	1	0	0	0	0	0	0
Nck	1	0	0	0	0	0	0
DOCK180	1	0	0	0	0	0	0
Rac	1	0	0	0	0	0	0
Tiam	1	0	0	0	0	0	0
RalGDS	0.916	0	0	0	0	0	0
AND_3_4	1	0	0	0	0	0	0
Ral	0.914	0	0	0	0	0	0
RalBP1	0.914	0	0	0	0	0	0
Cdc42	1	0	0	0	0	0	0
NIK	1	0	0	0	0	0	0
Talin	0.979	1	1	1	1	1	1
ILK	1	0	0	0	0	0	0
Arp_2_3	1	0	0	0	0	0	0
Pix_Cool	1	0	0	0	0	0	0
PAK	1	0	0	0	0	0	0
WASP	1	0	0	0	0	0	0
Graf	1	0	0	0	0	0	0
MLCK	0.998	0	0	0	0	0	0
MLCP	0.945	1	1	1	1	1	1
IL1_TNFR	1	0	0	0	0	0	0
Trafs	1	0	0	0	0	0	0
GCK	1	0	0	0	0	0	0
Gab1	1	0	0	0	0	0	0
Tab_1_2	1	0	0	0	0	0	0
Mekk1	1	0	0	0	0	0	0
Mekk2	1	0	0	0	0	0	0
Mekk3	1	0	0	0	0	0	0
Mekk4	1	0	0	0	0	0	0
ASK1	1	0	0	0	0	0	0
Trx	1	0	0	0	0	0	0
TAK1	1	0	0	0	0	0	0
Tpl2	1	0	0	0	0	0	0
MLK1	1	0	0	0	0	0	0
MLK2	1	0	0	0	0	0	0
MLK3	1	0	0	0	0	0	0

TAO_1_2	1	0	0	0	0	0	0
Sek1	1	0	0	0	0	0	0
MKK7	1	0	0	0	0	0	0
MKK3	1	0	0	0	0	0	0
MKK6	1	0	0	0	0	0	0
SAPK	1	0	0	0	0	0	0
p38	1	0	0	0	0	0	0
p90RSK	1	0	0	0	0	0	0
PP2A	1	1	1	1	1	1	1
SHP2	1	0	0	0	0	0	0
MKPs	1	0	0	0	0	0	0
PTEN	1	0	0	0	0	0	0
PTP1b	1	1	1	1	1	1	1
PTPPEST	1	0	0	0	0	0	0
PTPa	1	0	0	0	0	0	0
PLD	0.995	1	1	1	1	1	1
PA	0.995	1	1	1	1	1	1
ARF	0.995	1	1	1	1	1	1
DGK	1	0	0	0	0	0	0
B_Parvin	1	0	0	0	0	0	0
alpha_i_R	0.998	0	0	0	0	0	0
alpha_q_R	0.899	0	0	0	0	0	0
alpha_12_13_R	0.998	0	0	0	0	0	0
Ga_12_13	0.907	0	0	0	0	0	0
Gbg_i	1	0	0	0	0	0	0
Gbg_q	0.924	0	0	0	0	0	0
Gbg_12_13	0.907	0	0	0	0	0	0
PDE4	0.916	0	0	0	0	0	0
Cbp	0.984	0	0	0	0	0	0
IP3R1	0.998	0	0	0	0	0	0
Raf_DeP	0.514	0	1	0	0	1	0
PKC_primed	1	1	1	1	1	1	1
Raf_Loc	0.771	1	1	1	1	1	1
Raf_Rest	0.628	1	1	0	1	1	0
Palpha_s_R	1	0	0	0	0	0	0
Palpha_q_R	0.916	0	0	0	0	0	0
Palpha_i_R	1	0	0	0	0	0	0
Palpha_12_13_R	1	0	0	0	0	0	0
EGF	1	0	0	0	0	0	0

ECM	1	0	0	0	0	0	0
alpha_q_lig	1	0	0	0	0	0	0
alpha_i_lig	1	0	0	0	0	0	0
alpha_s_lig	1	0	0	0	0	0	0
alpha_12_13_lig	1	0	0	0	0	0	0
Stress	1	0	0	0	0	0	0
IL1_TNF	1	0	0	0	0	0	0
ExtPump	1	0	0	0	0	0	0

Supplementary Table S9. Comparison of the control kernel, driver node set, driver node set on switchboard dynamics (SBD), and optimal sensor set of the human fibroblast signaling network. In the table, ‘1’ indicates that the node in the corresponding row belongs to the group of the corresponding column, and ‘0’ indicates that the node in the corresponding row does not belong to the group of the corresponding column. Since the set of the driver nodes are not unique, the union and intersection of the sets obtained from 1,000 repetitions are considered.

Node name	Control kernel	Driver node set		Driver node set on SBD	Optimal sensor set
		Union	Intersection		
AA	0	0	0	1	0
AC	0	1	0	0	0
AND_3_4	0	1	0	0	0
ARF	0	1	0	1	0
ASK1	0	1	0	1	0
Actin	0	0	0	0	0
Akt	0	1	0	0	0
Arp_2_3	0	0	0	0	0
B_Arrestin	0	0	0	1	0
B_Parvin	0	1	0	0	0
Ca	0	0	0	1	0
CaM	0	1	0	1	0
CaMK	0	1	0	0	0
CaMKK	0	1	0	0	0
Cas	0	1	0	1	0
Cbp	0	1	0	0	0
Cdc42	0	0	0	1	0
Crk	0	1	0	0	0
Csk	0	0	0	0	0
DAG	1	0	0	0	0
DGK	0	1	0	0	0
DOCK180	0	1	0	0	0
EGFR	0	1	0	1	0

Erk	0	0	0	1	0
Fak	0	1	0	1	0
GCK	0	1	0	0	0
GRK	0	1	0	0	0
Ga_12_13	0	0	0	0	0
Gab1	0	1	0	0	0
Gai	0	1	0	0	0
Gaq	0	1	0	0	0
Gas	0	1	0	0	0
Gbg_12_13	0	1	0	1	0
Gbg_i	0	1	0	1	0
Gbg_q	0	1	0	1	0
Gbg_s	1	1	0	0	0
Graf	0	1	0	0	0
Grb2	0	1	0	1	0
IL1_TNFR	0	1	1	1	0
ILK	0	1	0	1	0
IP3	0	1	0	0	0
IP3R1	0	0	0	0	0
Integrins	0	1	0	0	0
MKK3	0	0	0	0	0
MKK6	0	0	0	0	0
MKK7	0	0	0	0	0
MKPs	0	1	0	0	0
MLCK	0	1	0	0	0
MLCP	0	1	0	0	0
MLK1	0	1	0	1	0
MLK2	0	1	0	0	0
MLK3	0	1	0	1	0
Mek	0	0	0	0	0
Mekk1	0	0	0	0	0
Mekk2	0	0	0	0	0
Mekk3	0	1	0	0	0
Mekk4	0	1	0	1	0
Myosin	0	0	0	0	0
NIK	0	0	0	0	0
Nck	0	1	0	1	0
PA	0	0	0	1	0
PAK	0	1	0	0	0
PDE4	0	1	0	0	0

PDK1	0	1	0	1	0
PI3K	0	1	0	0	0
PI4K	0	1	0	0	0
PI5K	0	1	0	0	0
PIP2_34	0	1	0	1	0
PIP2_45	1	1	0	1	0
PIP3_345	0	1	0	1	0
PIP_4	1	0	0	0	1
PKA	0	1	0	1	0
PKC	0	1	0	1	0
PKC_primed	1	1	0	0	0
PLA2	0	1	0	0	0
PLC_B	0	1	0	1	0
PLC_g	0	1	0	0	0
PLD	0	0	0	0	0
PP2A	0	1	0	1	0
PTEN	0	0	0	1	0
PTP1b	0	1	0	1	0
PTPPEST	0	1	0	0	0
PTPa	0	1	0	0	0
Palpha_12_13_R	0	1	0	0	0
OPalpha_i_R	0	1	0	1	0
Palpha_q_R	0	1	0	0	0
Palpha_s_R	0	1	0	0	0
Pix_Cool	0	0	0	0	0
RGS	0	1	0	1	0
RKIP	0	1	0	1	0
Rac	0	0	0	0	0
Raf	0	1	0	0	0
Raf_DeP	1	1	0	0	0
Raf_Loc	1	1	0	0	0
Raf_Rest	0	1	0	0	0
Ral	0	0	0	0	0
RalBP1	0	0	0	1	0
RalGDS	0	1	0	0	0
Rap1	0	1	0	0	0
Ras	0	0	0	1	0
RasGRF_GRP	0	1	0	0	0
Rho	1	0	0	1	0
RhoGDI	0	1	0	0	0

RhoK	0	1	0	1	0
SAPK	0	0	0	0	0
SHP2	0	1	0	1	0
Sek1	0	0	0	0	0
Shc	0	1	0	0	0
Sos	0	1	0	0	0
Src	0	0	0	1	0
TAK1	0	0	0	1	0
TAO_1_2	0	1	1	1	0
Tab_1_2	0	1	0	0	0
Talin	0	1	0	1	0
Tiam	0	1	0	0	0
Tpl2	0	1	0	1	0
Trafs	0	1	0	1	0
Trx	0	1	0	1	0
Vinc	0	0	0	0	1
WASP	0	1	0	0	0
alpha_12_13_R	1	0	0	1	0
alpha_i_R	0	1	0	1	0
alpha_q_R	1	1	0	1	0
alpha_s_R	1	0	0	1	0
cAMP	1	0	0	1	0
p115RhoGEF	0	1	0	0	0
p120RasGAP	0	1	0	0	0
p190RhoGAP	0	0	0	0	0
p38	0	0	0	0	0
p90RSK	0	1	0	0	0

IV. Supplementary References

1. J. Kim, T. G. Kim, S. H. Jung, J. R. Kim, T. Park, P. Heslop-Harrison, K. H. Cho, Evolutionary design principles of modules that control cellular differentiation: consequences for hysteresis and multistationarity. *Bioinformatics* **24**, 1516 (2008).
2. F. Li, T. Long, Y. Lu, Q. Ouyang, C. Tang, The yeast cell-cycle network is robustly designed. *Proc Natl Acad Sci U S A* **101**, 4781 (2004).
3. A. Abdi, M. B. Tahoori, E. S. Emamian, Fault diagnosis engineering of digital circuits can identify vulnerable molecules in complex cellular pathways. *Sci Signal* **1**, ra10 (2008).